Removal of Atmospheric Effects from AVHRR Albedos

PETER KOEPKE

Universitaet Muenchen, Meteorologisches Institut, Muenchen, Federal Republic of Germany

17 March 1989 and 10 July 1989

ABSTRACT

Based on numerical simulations, coefficients are determined to be used in a linear relationship between clear-sky planetary albedo and surface albedo. These coefficients are given as functions of solar zenith angle and atmospheric parameters for both the AVHRR (Advanced Very High Resolution Radiometer) channels 1 and 2 separately. The atmospheric effects in these channels are systematically different, because of the different spectral behavior of atmospheric parameters. Accordingly the use of the narrowband coefficients will improve the determination of surface properties from AVHRR data, compared with analogous methods using broadband coefficients.

1. Introduction

In order to derive surface albedo from planetary albedo, the latter must be corrected for atmospheric effects. This can be accomplished by applying radiative transfer models. However, it is often sufficient to use the simple linear relationship

$$\rho_t = a + b\rho_s \tag{1}$$

between the clear-sky albedo at the top of the atmosphere, ρ_t, and the surface albedo, ρ_s, rather than to carry out time-consuming radiative calculations.

Coefficients a and b are available for the total albedo, i.e., values integrated over the complete solar spectral range (e.g., Preuss and Geleyn 1980; Chen and Ohring 1984; and Koepke and Kriebel 1987). In this paper, coefficients a_i and b_i are presented for the narrowband shortwave channels of AVHRR (Advanced Very High Resolution Radiometer on NOAA satellites), where i denotes the channels 1 and 2. These channels provide the possibility for the narrow-to-broadband conversion necessary to derive the broadband albedo from satellite measured albedos (Wydick et al. 1987). Indeed, the AVHRR channels have been used recently by Zhong and Li (1988) and by Gutman (1988) to derive the albedo of land surfaces. In both these papers, Eq. (1) is used for the atmospheric correction, but with broadband coefficients. This is possible, since the wavelength conversion has been made previously. However, the atmospheric influence is completely different in both channels due to the different spectral behavior of the different atmospheric components. Therefore, separate atmospheric corrections for each channel should improve the results. Other research areas where channel dependent coefficients a_i and b_i could be of value are the use of AVHRR measured radiances to determine subpixel cloudiness (Saunders and Kriebel 1988), or vegetation indices (e.g., Duggin and Piwinski 1984).

2. Theory

For an arbitrary atmospheric column, the flux of solar radiation incident at the top of the atmosphere, E_t, will either be reflected back to space, absorbed by the atmosphere, or will penetrate into the ground. Thus, the solar radiation budget equation is

$$E_t = \rho_t E_t + E_{\text{abs}} + E_s(1 - \rho_s) \tag{2}$$

where E_{abs} is the flux absorbed within the atmosphere and E_s is the flux irradiating the surface (sun plus diffuse sky radiation).

For clear-sky conditions, the relationship between the albedo at the top of the atmosphere and the surface albedo, shown in Eq. (1), can be derived from Eq. (2) with

$$a = (E_t - E_s - E_{\text{abs}})/E_t \tag{3}$$

and

$$b = E_s/E_t. \tag{4}$$

It follows, that the simple Eq. (1) really describes radiation processes in the atmosphere. The coefficient a represents the relative amount of radiation scattered back to space by molecules and aerosol particles, and the coefficient b describes the flux-transmittance of the clear-sky atmosphere.

Corresponding author address: Dr. Peter Koepke, Meteorologisches Institut Universitaet Muenchen, Theresienstrasse 37, D-8000 Muenchen 2, F. R. Germany.

3. Model

Coefficients a_i and b_i are calculated as intercept and slope of a linear regression, made for a set of surface and planetary albedos that are calculated for different model atmospheres. This procedure is described in Koepke and Kriebel (1987) together with the radiative transfer model and atmospheric parameters used. However, in contrast to that paper, here the calculated fluxes are weighted with the relative spectral response of the AVHRR channels. The step function values used (Table 1) are valid for the radiometer on NOAA 7, but the spectral responses of the other AVHRRs are similar.

To get coefficients a_i and b_i, spectral radiances are calculated upward emerging at the top of the atmosphere and both upward and downward at the bottom of the atmosphere, by a successive-orders-of scattering program (Quenzel 1978) which accounts for all orders of scattering. The earth surfaces are taken into account by their spectral bidirectional reflection functions. The absorption by ozone obeys the Bouguer–Lambert law in each spectral interval and is accounted for in this way with absorption coefficients from Duetsch (1970). The absorption by water vapor, carbon dioxide and oxygen is handled by the exponential series method (e.g., Bakan et al. 1978) with values of the water vapor band absorption calculated as in Moskalenko (1969) with coefficients from Koepke and Quenzel (1978). The integration over wavelength is done according to Koepke (1982), being slightly modified to take into account the properties of the radiometer channels: The optical properties of the scattering particles and of the reflection functions vary slowly with wavelength. Thus, radiances are calculated with a value of the solar irradiance of 1 at wavelengths 0.44, 0.55, 0.67, 0.81, 1.01 μm and interpolated to get radiances at wavelength with $\Delta\lambda = 0.05$ μm. Finally, the true irradiance of the sun (Neckel and Labs 1981) and the relative spectral response of the AVHRR channels (Table 1) are taken into account, and the integration over wavelength is performed to get radiances for these channels. In each case, the radiances are calculated at 25 zenith angles and 80 azimuth angles and directly integrated over the hemisphere to get irradiances. From these flux densities, together with the weighted solar irradiance at the top of the atmosphere, the albedos both at the top of the atmosphere and at the surface are calculated for AVHRR channels 1 and 2, respectively. From a set of ρ_t and ρ_s, derived for the model atmospheres described in the following, the coefficients a_i and b_i are calculated as intercept and slope of a linear regression [Eq. (1)].

TABLE 1. Relative response τ of AVHRR channels 1 and 2 used for the calculations.

Channel 1		Channel 2	
λ (μm)	τ	λ (μm)	τ
0.5125–0.5375	0	0.6375–0.6625	0
0.5375–0.5625	0.03	0.6625–0.6875	0.01
0.5625–0.5875	0.55	0.6875–0.7125	0.14
0.5875–0.6125	0.78	0.7125–0.7375	0.73
0.6125–0.6375	0.93	0.7375–0.7625	0.99
0.6375–0.6625	0.96	0.7625–0.7875	0.99
0.6625–0.6875	0.84	0.7875–0.8125	0.94
0.6875–0.7125	0.19	0.8125–0.8375	0.87
0.7125–0.7375	0.04	0.8375–0.8625	0.87
0.7375–0.7625	0.01	0.8625–0.8875	0.87
0.7625–0.7875	0.01	0.8875–0.9125	0.85
0.7875–0.8125	0	0.9125–0.9375	0.81
		0.9375–0.9625	0.77
		0.9625–0.9875	0.66
		0.9875–1.0125	0.31
		1.0125–1.0375	0.07
		1.0375–1.0625	0.02
		1.0625–1.0875	0

The model atmospheres are assumed to be cloud free. The spectral optical depth of the air molecules (Young 1981) is taken into account with a barometric pressure of 1013 mb. Two aerosol types are considered, continental and maritime, for relative humidity of 70% (after Haenel and Bullrich 1978). For both types the refractive index varies with wavelength and both types are slightly absorbing—similar to the SRA continental aerosol model. The aerosol load is simulated as clear and turbid atmosphere, with spectral Linke turbidity factors at 0.55 μm of $T_{.55} = 1.5$ and 5, respectively. The corresponding spectral aerosol optical depths, $\delta_{.55}$, are 0.05 and 0.4. The aerosol scale height is assumed to be 1.2 km. The total amount of ozone is varied with values 0.24 and 0.36 cm NTP O_3 (van Heuklon 1979). The amount of water vapor in the vertical column is chosen with values of 0.5, 2, and 5 g cm^{-2}, a range which covers the conditions in the earth's atmosphere (Tuller 1968). To describe the earth surface variability, the following spectral bidirectional reflection functions are used in the study: clean, fresh fallen snow with spectral values from Kondratiev (1969) and pasture land, savannah, and coniferous forest after Kriebel (1978). The solar zenith angle is varied with 12.5°, 32.5°, 57.5° and 72.5°, as indicated in Figs. 1 and 2. The coefficients for other angles are determined by a natural spline interpolation.

4. Results

The coefficients a_i and b_i of Eq. (1), where i denotes the AVHRR channels 1 and 2, are presented in Figs. 1 and 2 with dashed lines for clear atmosphere (spectral aerosol optical depth $\delta_{.55} = 0.05$) and with solid lines for turbid atmosphere ($\delta_{.55} = 0.4$). Also varied is the amount of absorbing gases. Ozone influences the radiation field in channel 1 and water vapor (together with a fixed amount of oxygen) in channel 2. Thus in Fig. 1 the curves valid for different turbidity are separated for low and high ozone amount (0.24 and 0.36 cm NTP). In Fig. 2 the curves are separated for three

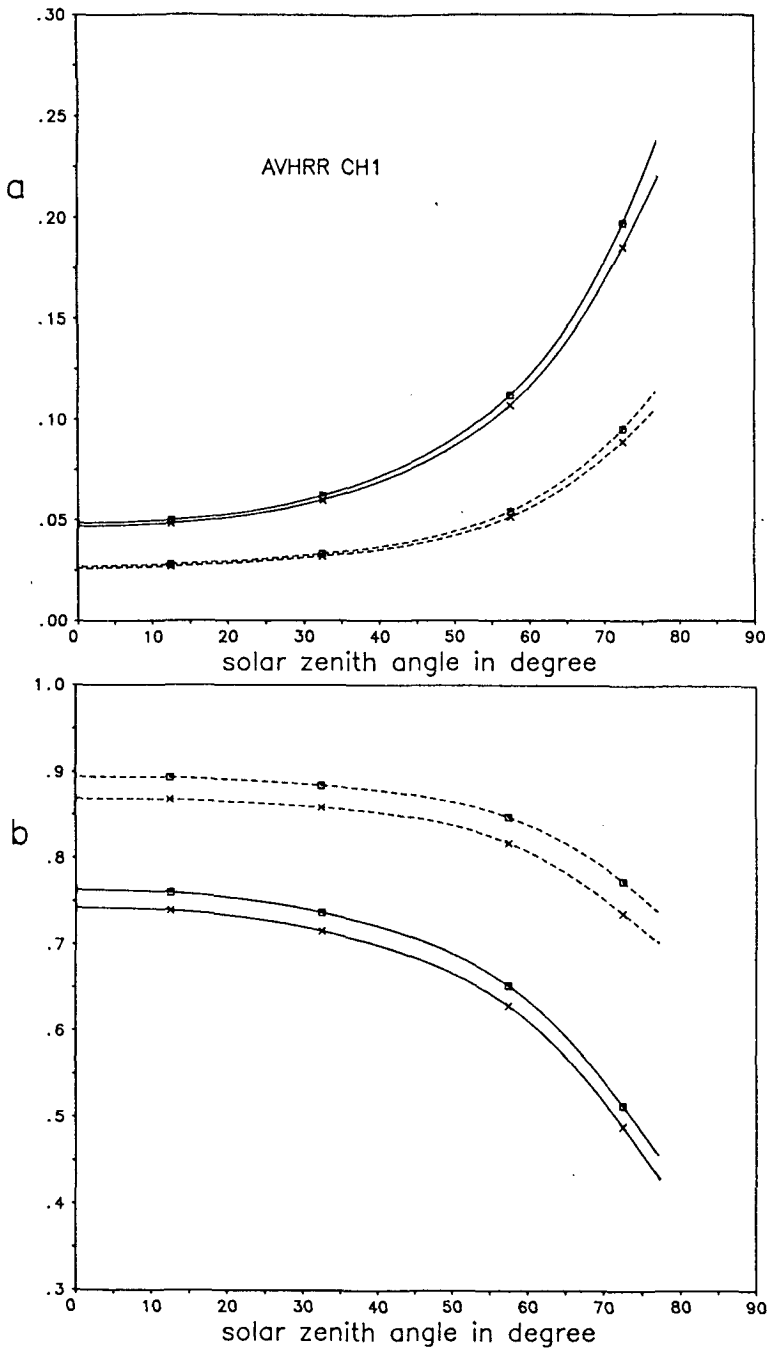

FIG. 1. Coefficients a and b for the linear relation [Eq. (1)] between planetary and surface albedo that are weighted with the spectral response of AVHRR channel 1. Shown are values as function of solar zenith angle for a clear atmosphere (aerosol optical depth $\delta_{.55} = 0.05$, dashed lines) and for a turbid atmosphere ($\delta_{.55} = 0.4$; solid lines). The ozone amount is varied with 0.24 cm STP (square symbols) and 0.36 cm STP (crosses).

examples of atmospheric water vapor content (0.5, 2 and 5 g cm^{-2}).

For both channels, i.e., in both figures, the coefficients a_i increase with increasing solar zenith angle and with increasing turbidity, since both effects increase the amount of upward scattered photons. The values for channel 2 are lower than those for channel 1, due to the decrease of the spectral optical depth with in-

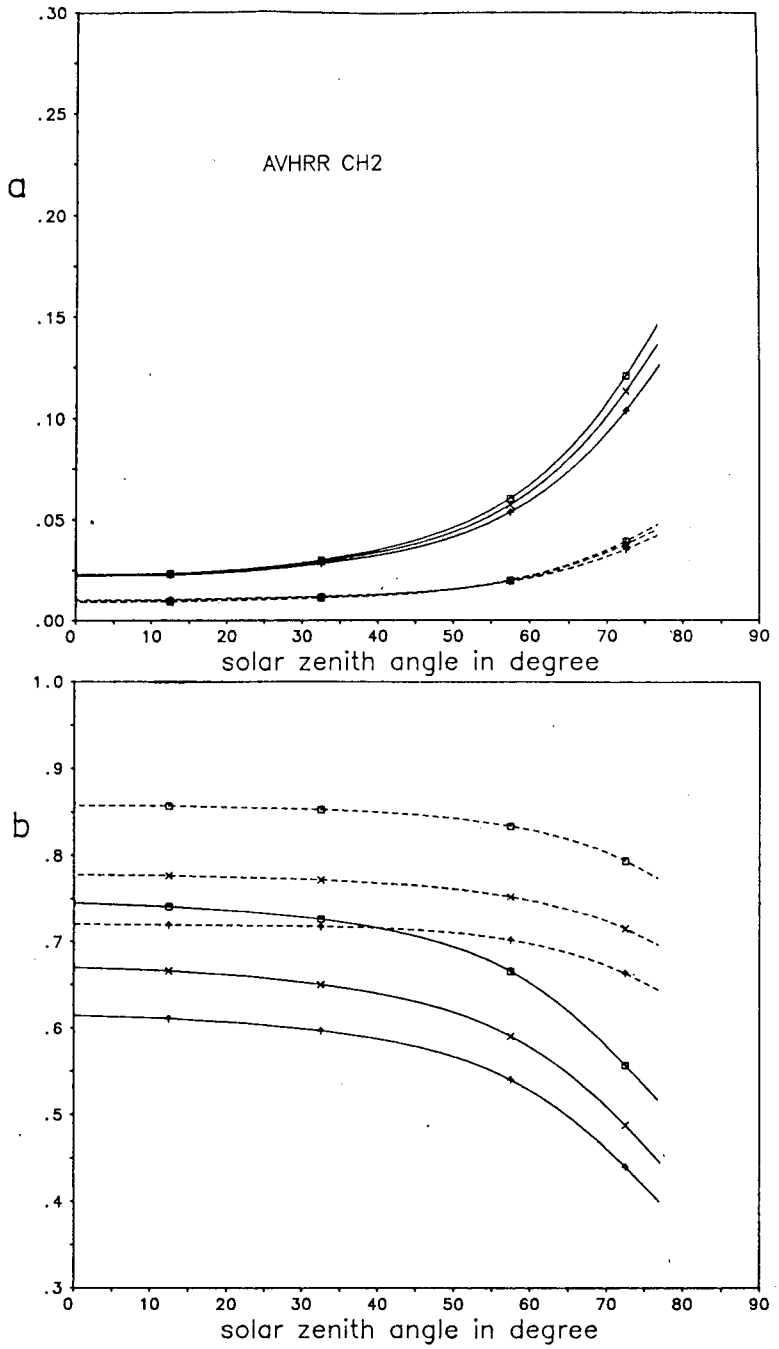

FIG. 2. Coefficients a and b for AVHRR channel 2. Solar zenith angle and atmospheric turbidity are as in Fig. 1. But the gaseous absorber varied is water vapor with 0.5 g cm^{-2} (square symbols), 2 g cm^{-2} (crosses), and 5 g cm^{-2} (arrows).

creasing wavelength as well as a slight decrease of the single scattering albedo of both aerosol types used.

The absorbing gases reduce the amount of scattered photons and thereby the a_i-coefficients. In channel 1 this reduction increases with solar zenith angle due to the increasing optical path through the ozone layer. In channel 2 the reduction of the a-coefficients due to water vapor is low, since water vapor is a weak absorber below 1 μm and absorbs only in parts of the spectral range of the channel. Accordingly, the coefficients a_2 are very close together for different amounts of water vapor. The pathlengths of the scattered photons increase with solar zenith angle (Bakan and Quenzel 1976) and so consequently does the water vapor ab-

sorption, resulting in the fact that the reduction of the a_2-coefficients due to water vapor increases with solar zenith angle. For low turbidity and high sun, the a_2-coefficients are not only nearly equal, but even interchanged. This effect results from the procedure determining the coefficients as intercept of a linear fit made with albedo values for different surface types. For snow the effectiveness of water vapor absorption within the channel is higher than for other land surfaces due to the different spectral dependence of their albedos within the spectral range of the channel. Thus, for high content of water vapor the linear regression is supported with relatively low planetary albedos at high surface albedos, resulting in the relatively high intercept, and vice versa.

TABLE 2. Coefficients a_i and b_i for solar zenith angle θ_0 in degree, aerosol optical depth at .55 μm, $\delta_{.55}$, ozone amount, u_{O_3} in cm NTP, and water vapor, u_{H_2O} in g cm^{-2}.

Channel 1

θ_0	$\delta_{.55}$	u_{O_3}	a_1	b_1	u_{O_3}	a_1	b_1
0	0.05	0.24	.027	.895	0.36	.026	.870
10			.028	.894		.027	.869
20			.030	.892		.029	.866
30			.033	.887		.031	.860
40			.037	.879		.035	.853
50			.044	.867		.042	.839
60			.059	.839		.056	.808
70			.086	.791		.081	.754
75			.106	.755		.098	.719
80			.129	.713		.118	.679
0	0.4	0.24	.049	.763	0.36	.047	.743
10			.050	.761		.048	.741
20			.053	.754		.051	.734
30			.060	.741		.058	.720
40			.071	.722		.069	.700
50			.090	.691		.086	.668
60			.122	.636		.116	.612
70			.178	.543		.168	.519
75			.218	.483		.203	.458
80			.265	.420		.244	.393

Channel 2

θ_0	$\delta_{.55}$	u_{H_2O}	a_2	b_2	u_{H_2O}	a_1	b_2	u_{H_2O}	a_2	b_2
0	0.05	0.5	.009	.858	2.0	.010	.778	5.0	.010	.720
10			.009	.857		.010	.777		.010	.719
20			.010	.856		.010	.775		.011	.718
30			.011	.854		.011	.773		.012	.717
40			.012	.850		.013	.769		.013	.715
50			.015	.843		.015	.762		.015	.710
60			.022	.830		.022	.749		.021	.698
70			.035	.804		.034	.724		.032	.672
75			.044	.783		.042	.705		.039	.652
80			.054	.757		.051	.680		.047	.628
0	0.4	0.5	.023	.746	2.0	.023	.670	5.0	.022	.615
10			.023	.743		.023	.667		.022	.612
20			.025	.737		.025	.661		.024	.606
30			.028	.728		.028	.652		.027	.599
40			.035	.717		.033	.640		.032	.588
50			.046	.695		.044	.619		.041	.568
60			.067	.652		.064	.578		.060	.528
70			.108	.579		.101	.509		.093	.461
75			.135	.534		.126	.465		.116	.418
80			.167	.484		.156	.416		.143	.370

TABLE 3. Coefficients a_i and b_i for cosine solar zenith angle $\mu = \cos\theta_0$[9] aerosol optical depth at .55 μm, $\delta_{.55}$, ozone amount, u_{O_3} in cm NTP, and water vapor, u_{H_2O} in g cm^{-2}.

Channel 1

μ	$\delta_{.55}$	u_{O_3}	a_1	b_1	u_{O_3}	a_1	b_1
1.	0.05	0.24	.027	.895	0.36	.026	.870
.95			.029	.892		.028	.867
.9			.031	.889		.030	.863
.85			.033	.885		.032	.859
.8			.035	.882		.034	.856
.75			.037	.878		.036	.852
.7			.040	.874		.038	.847
.65			.044	.867		.041	.840
.6			.048	.860		.045	.832
.55			.053	.851		.050	.821
.5			.059	.839		.056	.808
.45			.066	.827		.063	.793
.4			.075	.812		.070	.776
.35			.084	.794		.079	.757
.3			.096	.774		.089	.737
.25			.108	.751		.100	.715
.2			.121	.727		.112	.693
1.	0.4	0.24	.049	.763	.036	.047	.743
.95			.052	.756		.050	.736
.9			.057	.747		.055	.726
.85			.062	.738		.059	.717
.8			.067	.730		.064	.708
.75			.073	.720		.069	.698
.7			.080	.709		.076	.687
.65			.088	.695		.084	.673
.6			.098	.678		.093	.656
.55			.109	.659		.104	.637
.5			.122	.636		.116	.612
.45			.137	.609		.131	.586
.4			.155	.580		.147	.557
.35			.175	.548		.166	.524
.3			.198	.514		.186	.490
.25			.224	.477		.208	.452
.2			.251	.440		.230	.415

Channel 2

μ	$\delta_{.55}$	u_{H_2O}	a_2	b_2	u_{H_2O}	a_2	b_2	u_{H_2O}	a_2	b_2
1.	0.05	0.5	.009	.858	2.0	.010	.778	5.0	.010	.720
.95			.010	.856		.010	.776		.011	.719
.9			.010	.855		.011	.774		.011	.718
.85			.011	.853		.011	.772		.012	.717
.8			.012	.852		.012	.770		.012	.716
.75			.013	.850		.013	.768		.013	.715
.7			.014	.847		.014	.766		.014	.714
.65			.015	.844		.015	.763		.015	.711
.6			.017	.840		.017	.759		.017	.708
.55			.019	.835		.019	.754		.019	.703
.5			.022	.830		.022	.749		.021	.698
.45			.026	.823		.025	.743		.024	.691
.4			.030	.815		.029	.735		.027	.684
.35			.034	.806		.033	.726		.031	.674
.3			.039	.794		.038	.715		.035	.663
.25			.045	.780		.043	.702		.040	.650
.2			.051	.765		.048	.689		.045	.637

TABLE 3. (*Continued*)

		Channel 2								
μ	$\delta_{.55}$	u_{H_2O}	a_2	b_2	u_{H_2O}	a_2	b_2	u_{H_2O}	a_2	b_2
1.	0.4	0.5	.023	.746	2.0	.023	.670	5.0	.022	.615
.95			.024	.739		.024	.663		.024	.608
.9			.027	.732		.027	.657		.026	.603
.85			.030	.727		.030	.651		.028	.598
.8			.032	.721		.031	.645		.030	.593
.75			.035	.715		.034	.639		.033	.587
.7			.039	.708		.037	.631		.036	.580
.65			.044	.698		.042	.621		.040	.571
.6			.050	.686		.048	.609		.045	.559
.55			.058	.670		.055	.595		.052	.545
.5			.067	.652		.064	.578		.060	.528
.45			.078	.631		.074	.559		.068	.509
.4			.091	.608		.086	.537		.079	.488
.35			.105	.583		.099	.514		.090	.465
.3			.123	.557		.113	.488		.104	.440
.25			.139	.529		.129	.460		.119	.413
.2			.157	.501		.146	.432		.134	.386

If only surfaces without snow are taken into account to determine a_2-coefficients, the latter decrease, with increasing water vapor for all solar zenith angles, as expected. In this case, the a_2-values are changed for high sun on the order of 0.001 for low and 0.002 for high turbidity.

The behavior of the b-coefficients is similar also in both channels, i.e., in Figs. 1 and 2. The coefficients, which describe the flux-transmittances, decrease with increasing solar zenith angle, with increasing turbidity, and with increasing amounts of gaseous absorbers. Like a beam-transmittance, given as negative exponent of the optical depth within the optical path, the coefficients b decrease most strongly for high turbidity in combination with increasing solar zenith angle. However, the b-coefficients are always greater than the corresponding beam-transmittances for the direct sun, since the sky radiance increases the transmitted flux. The relative amount of sky radiance increases with solar zenith angle and turbidity, with the result that the variation of b with solar zenith angle is relatively slight up to high zenith angles.

In channel 1, ozone reduces the transmission, independent of turbidity, and the reduction increases with solar zenith angle. This effect, which is shown in Fig. 1 for b-values at low turbidity, is masked for high turbidity due to the transmittance which is already low; therefore further reduction results only in small absolute differences. In channel 2 the reduction of b with increasing water vapor from 0.5 to 2 g cm^{-2} is similar to that from 2 to 5 g cm^{-2}, as a consequence of saturation effects in the band absorption. The water vapor absorption is proportional to the path length of photons as they travel through the atmosphere. At high and medium sun the mean path length of the downward scattered photons is longer than that of the unscattered photons, but it is shorter at low sun (Bakan and Quenzel 1976). Thus, at low sun, both direct sun and sky radiance are similarly reduced by water vapor, whereas at high sun a relatively greater amount of sky radiation is absorbed. Therefore, the increase of the flux-transmittance compared to the beam-transmittance is reduced by water vapor relatively more strongly for high than for low sun. This results in a slight variation of b_2 with solar angle, which is even more pronounced than for b_1.

Numerical values of the coefficients are given in Table 2 for solar zenith angles in 10-degree steps and in Table 3 for cosine of solar zenith angle, $\cos\theta_0 = \mu$, in steps of $\Delta\mu = 0.05$. These values are calculated by a spline routine from the values directly determined from multiple scattering calculations. To work with AVHRR data in wintertime in subpolar latitudes it is necessary to take into account solar zenith angles up to 80 degrees. Consequently values for this angle are extrapolated and presented in Table 2, even though the multiple scattering code is not used for such a low sun due to effects of the spherical shell of the atmosphere.

5. Conclusion

Coefficients a and b are valid for aerosol types used in the derivation; for others they might be erroneous. For actual aerosols that may be different (e.g., with respect to their absorption) the atmospheric masking effects would also be different (e.g., Herman and Browing 1975; Koepke and Kriebel 1987), and consequently the corresponding a- and b-values. Also the spectral behavior of the albedo types used to calculate the coefficients may have a small influence on the a_i-

and b_i-values. This results from the spectral structure of water vapor absorption. Its influence on the spectrally integrated albedos at the top of the atmosphere is different for surface albedos with different spectral distribution, but with the same value integrated over the wavelength region.

Thus, the coefficients presented here do not allow one to correct for atmospheric masking precisely in any actual case. However, the aerosol types used to derive the coefficients are valid for average continental conditions. Moreover, coefficients a and b, calculated with respect to other aerosol properties than the optical depth, would not be helpful since usually no actual measurements of such atmospheric parameters are available. Values of horizontal visibility and dewpoint, however, are routinely measured at many places. These values (converted to optical depth and water vapor content, respectively) provide the knowledge of atmospheric properties which can be taken into account to decide between the coefficients given in this paper.

The results highlight the fact that atmospheric effects in the two solar AVHRR channels have strong systematic differences. Therefore, the given narrowband a_i- and b_i-coefficients, which allow separate atmospheric corrections for each channel, will improve the determination of surface parameters compared with analogous calculations using broadband coefficients.

Acknowledgments. I would like to thank K. T. Kriebel for his encouragement to publish the results and W. Thomas and B. Vogel for computer work. The work was partly sponsored by the BMFT (German Research Minister) under Grant KF 1014/3.

REFERENCES

Bakan, S., and H. Quenzel, 1976: Path length distribution of photons scattered in turbid atmospheres. *Beitr. Phys. Atmos.*, **49**, 272–284.

——, P. Koepke and H. Quenzel, 1978: Radiation calculations in absorption bands: Comparison of exponential series and path length distribution-method. *Beitr. Phys. Atmos.*, **51**, 28–30.

Chen, T. S., and G. Ohring, 1984: On the relationship between clear-sky planetary and surface albedos. *J. Atmos. Sci.*, **41**, 156–158.

Duetsch, H. U., 1970: Absorptionskoeffizienten des Ozons. F. Linke, F. Baur. Meteorolog. Taschenbuch, Band II, Akadem Verlags. Ges., Leipzig, 571 pp.

Duggin, M. J., and D. Piwinski, 1984: Recorded radiance indices for vegetation monitoring using NOAA AVHRR data: Atmospheric and other effects in multitemporal data sets. *Appl Opt.*, **23**, 2620–2623.

Gutman, G., 1988: A simple method for estimating monthly mean albedo of land surfaces from AVHRR data. *J. Appl. Meteor.*, **27**, 973–988.

Haenel, G., and K. Bullrich, 1978: Physico–chemical property models of trophospheric aerosol particles. *Beitr. Phys. Atmos.*, **51**, 129–138.

Herman, B. M., and S. R. Browing, 1975: The effect of aerosols on the Earth-atmosphere albedo. *J. Atmos. Sci.*, **32**, 1430–1445.

von Heuklon, T. K., 1979: Estimating atmospheric ozone for solar radiation models. *Sol. Energy*, **22**, 63–68.

Koepke, P., 1982: Meteosat-VIS-channel: Signal reduction due to atmospheric water vapor and ozone. *Beitr. Phys. Atmos.*, **55**, 358–369.

——, and H. Quenzel, 1978: Water vapor: Spectral transmission at wavelengths between 0.7 and 1 μm. *Appl. Opt.*, **17**, 2114–2118.

——, and K. T. Kriebel, 1987: Improvements in the shortwave cloudfree radiation budget accuracy. Part I: Numerical study including surface anisotropy. *J. Climate Appl. Meteor.*, **26**, 374–395.

Kondratiev, K. Y., 1969: *Radiation in the Atmosphere.* Academic Press.

Kriebel, K. T., 1978: Measured spectral bidirectional reflection properties of four vegetated surfaces. *Appl. Opt.*, **17**, 253–259.

Moskalenko, N. L., 1969: The spectral transmission function in the bands of the water-vapor, O_3, N_2O and N_2 atmospheric components. *Izv. Atmos. Oceanic Phys.*, **5**, 1179–1190.

Neckel, H., and D. Labs, 1981: Improved data of solar spectral irradiance from 0.33 to 1.25 μ. *Solar Phys.*, **74**, 231–242.

Preuss, H. J., and F. Geleyn, 1980: Surface albedos derived from satellite data and their impact on forecast models. *Arch. Meteor. Bioklim. Ser. A.*, **29**, 345–356.

Quenzel, H., 1978: Computation of luminance and color distribution in the sky. *Daylight Illumination-Color-Contrast Tables for Fullform Objects,* M. Nagel, Ed., Academic Press.

Saunders, R., and K. T. Kriebel, 1988: An improved method for detecting clear-sky and cloudy radiances from AVHRR data. *Int. J. Remote Sensing*, **9**, 123–150.

Tuller, S. E., 1968: World distribution of mean monthly and annual precipitable water. *Mon. Wea. Rev.*, **96**, 785–797.

Wydick, J. E., P. A. Davis and A. Gruber, 1987: Estimation of broadband planetary albedo from operational narrowband satellite measurements. NOAA Tech. Rep. NESDIS 27, U.S. Department of Commerce, 32 pp.

Young, A. T., 1981: On the Rayleigh-scattering optical depth of the atmosphere. *J. Appl. Meteor.*, **20**, 328–330.

Zhong, Q., and L. Yinhai, 1988: Satellite observation of surface albedo over the Quinghai-Yizang plateau region. *Adv. Atmos. Sci.*, **5**, 57–65.